

Article

Using Fission-Track Radiography Coupled with Scanning Electron Microscopy for Efficient Identification of Solid-Phase Uranium Mineralogy at a Former Uranium Pilot Mill (Grand Junction, Colorado)

Raymond H. Johnson ^{1,*}, Susan M. Hall ² and Aaron D. Tigar ¹

¹ RSI EnTech, LLC, U.S. Department of Energy Office of Legacy Management, 2597 Legacy Way, Grand Junction, CO 81503, USA; aaron.tigar@lm.doe.gov

² U.S. Geological Survey, MS 939, Denver Federal Center, P.O. Box 25046, Denver, CO 80225, USA; susanhall@usgs.gov

* Correspondence: ray.johnson@lm.doe.gov; Tel.: +1-970-248-6468

Abstract: At a former uranium pilot mill in Grand Junction, Colorado, mine tailings and some subpile sediments were excavated to various depths to meet surface radiological standards, but residual solid-phase uranium below these excavation depths still occurs at concentrations above background. The combination of fission-track radiography and scanning electron microscope energy-dispersive X-ray spectroscopy (SEM-EDS) provides a uniquely efficient and quantitative way of determining mineralogic associations of uranium that can influence uranium mobility. After the creation of sample thin sections, a mica sheet is placed on those thin sections and irradiated in a nuclear research reactor. Decay of the irradiated uranium creates fission tracks that can be viewed with a microscope. The fission-track radiography images indicate thin section sample areas with elevated uranium that are focus areas for SEM-EDS work. EDS spectra provide quantitative elemental data that indicate the mineralogy of individual grains or grain coatings associated with the fission-track identification of elevated uranium. For the site in this study, the results indicated that uranium occurred (1) with coatings of aluminum–silicon (Al/Si) gel and gypsum, (2) dispersed in the unsaturated zone associated with evaporite-type salts, and (3) sorbed onto organic carbon. The Al/Si gel likely formed when low-pH waters were precipitated during calcite buffering, which in turn retained or precipitated trace amounts of Fe, As, U, V, Ca, and S. Understanding these mechanisms can help guide future laboratory and field-scale efforts in determining long-term uranium release rates to groundwater.

Keywords: fission-track radiography; scanning electron microscope; uranium



Citation: Johnson, R.H.; Hall, S.M.; Tigar, A.D. Using Fission-Track Radiography Coupled with Scanning Electron Microscopy for Efficient Identification of Solid-Phase Uranium Mineralogy at a Former Uranium Pilot Mill (Grand Junction, Colorado). *Geosciences* **2021**, *11*, 294. <https://doi.org/10.3390/geosciences11070294>

Academic Editors: Maria Laura Balestrieri and Jesus Martinez-Frias

Received: 24 May 2021

Accepted: 9 July 2021

Published: 16 July 2021

Publisher's Note: MDPI stays neutral with regard to jurisdictional claims in published maps and institutional affiliations.



Copyright: © 2021 by the authors. Licensee MDPI, Basel, Switzerland. This article is an open access article distributed under the terms and conditions of the Creative Commons Attribution (CC BY) license (<https://creativecommons.org/licenses/by/4.0/>).

1. Introduction

Elevated solid-phase uranium concentrations can be determined using various traditional techniques, such as X-ray diffraction (XRD), X-ray fluorescence (XRF), gamma-ray spectroscopy, and solid-phase digestion. The resulting data provide a useful guide for the locations and depths of overall uranium contamination at legacy mill sites when completed on core samples across the site [1,2]. Except for direct uranium mineral identification with XRD, which is rare because discrete uranium minerals rarely form at the low uranium concentrations found at remediated sites, these techniques provide minimal direct evidence of mineralogic associations (e.g., sorption to precipitated iron) that could influence uranium mobility between solid and water phases. In addition, XRD and XRF are generally not sensitive enough to detect solid-phase uranium at lower concentrations (<15 milligrams per kilogram (mg/kg)) that are above background, but below radiological standards, which is typical of many areas of remediated uranium mill sites (e.g., [1,2]). Gamma-ray spectroscopy can provide solid-phase concentrations of multiple radionuclides (including uranium) by converting radiological properties to mass units, but it does not provide

information on mineralogic associations. Sequential extraction techniques can provide some information on uranium mineralogic associations using progressively stronger extractions fluids, but these associations are relatively qualitative without confirmation of what minerals or sorbing material actually exists [1,2].

Fission-track radiography identifies areas within a thin section that have elevated uranium concentrations [3–5]. For samples related to environmental contamination, fission-track radiography can detect uranium below the detection limit of scanning electron microscope energy-dispersive X-ray spectroscopy (SEM-EDS). Then, the mineralogy of the elevated uranium areas identified in fission-track radiography can be studied in detail using SEM-EDS. Thus, the combination of fission-track radiography and SEM-EDS provides a uniquely efficient and quantitative way to determine mineralogic associations of uranium that can influence uranium mobility. Understanding these solid-phase uranium mineralogic associations are an important step in determining potential uranium mobility mechanisms that can influence long-term groundwater quality at legacy uranium mill sites.

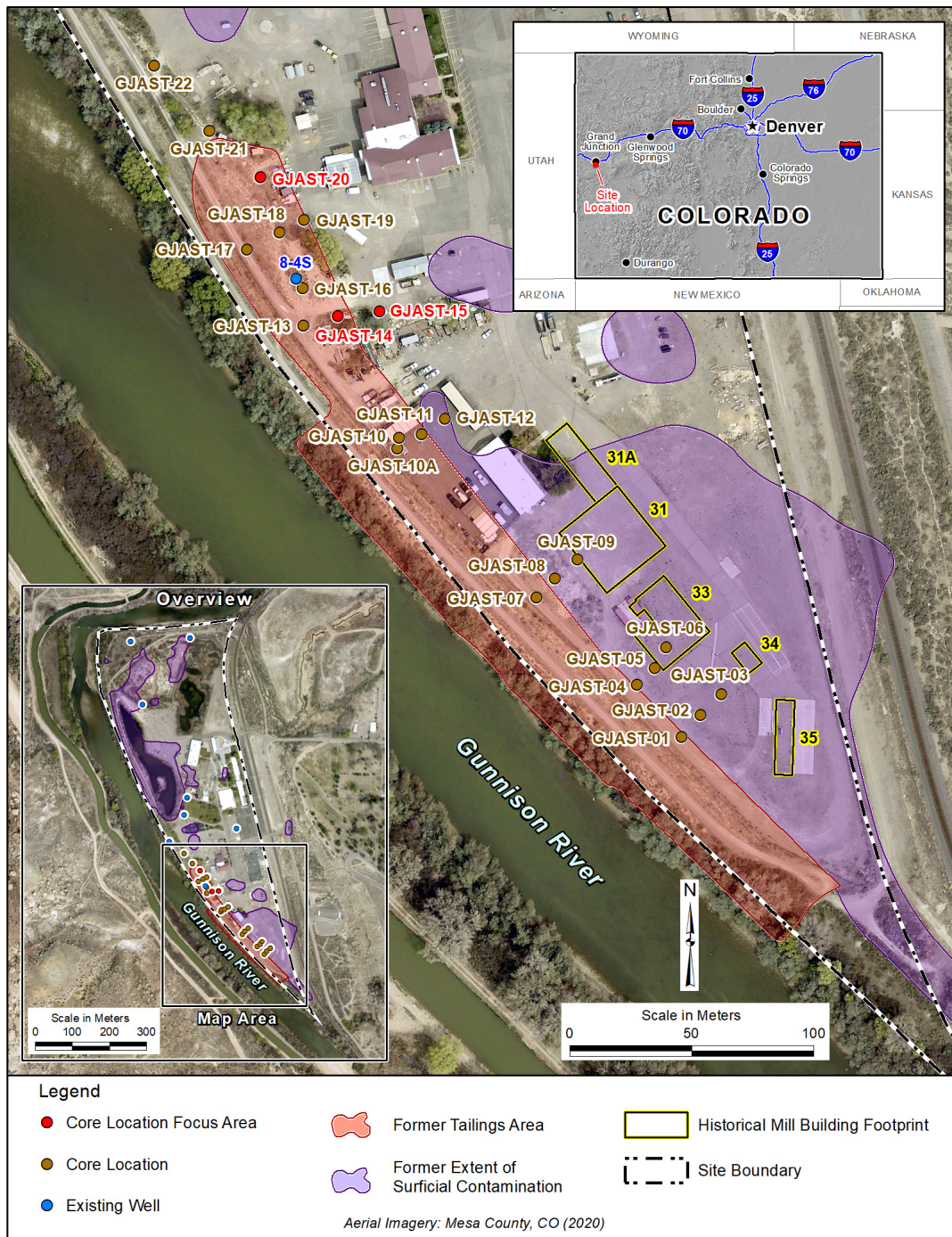
2. Program Background and Studied Site

The U.S. Department of Energy Office of Legacy Management (LM) oversees the long-term surveillance and maintenance (LTS&M) at multiple legacy uranium mill sites (<https://www.energy.gov/lm/sites/lm-sites>, accessed on 23 May 2021). At several LM sites, mine tailings and some subpile sediments were removed and excavated to various depths (generally less than 3 m (m)) to meet surface radiological standards (the concentration of radium –226 averaged over any area of 100 square meters shall not exceed the background level by more than (1) 0.185 becquerels per gram (Bq/g) (5 picocuries per gram (pCi/g)) averaged over the first 15 cm (cm) of soil below the surface, and (2) 0.555 Bq/g (15 pCi/g) averaged over 15 cm thick layers of soil more than 15 cm below the surface). However, residual solid-phase uranium usually occurs below these excavation depths at concentrations above background (the Grand Junction, Colorado, Site [1,6,7]; the Monticello, Utah, Disposal and Processing Sites [2]; and the Riverton, Wyoming, Processing Site [8,9]). At these sites, early conceptual and numerical models of uranium mobility considered uranium as moving at groundwater flow rates ([10] for the Grand Junction site) or having a retardation factor based only on sorption/desorption between the solid phase and groundwater without any additional residual solid-phase uranium sources ([11] for the Riverton site). Subsequent work has identified elevated solid-phase uranium concentrations below and downgradient of the former tailings areas that may be contributing to ongoing groundwater contamination [1,2,12,13]. As a consequence, natural attenuation and active remediation time frames of uranium plumes appear to be taking longer than originally predicted [12].

The LM Applied Studies and Technology (AS&T) Program develops applied science techniques that can be used to improve LTS&M efforts at multiple LM sites. To better understand the potential mineralogic controls on uranium release from former tailings subpile sediments, the AS&T Program developed a novel technique that couples fission-track radiography with SEM-EDS on thin sections for the efficient identification of solid-phase uranium associations. A similar approach was used by [14] that compared fission-track radiography and SEM-EDS microanalysis on soil particles from the Chernobyl Nuclear Power Plant. The authors of [14] completed these analyses on the soil particles directly without the creation of thin sections, and they were looking specifically at radioactive particles that created soil contamination.

Analyses were completed on solid-phase sediments from the Grand Junction office (GJO) site (GJO, Figure 1) where uranium in groundwater is still elevated, even after surface remediation. Prior work at the GJO site identified zones with elevated solid-phase uranium concentrations via sequential extraction and total digestion [1]. At the GJO site, uranium mill tailings were present for several decades before being removed to a disposal cell after excavation to depths that met radiological standards [6]. Available solid-phase concentration data are summarized below, and a more detailed site history, relevant site

documents, and LTS&M data reports can be found at <https://www.energy.gov/lm/grand-junction-colorado-site>, accessed on 23 May 2021. GJO site groundwater and surface water quality data can be accessed interactively at <https://gems.lm.doe.gov/#site=GJO>, accessed on 23 May 2021.



S3363602 07/07/2021 12:59:53 PM

Figure 1. GJO site map with coring locations [1] and former tailings area [10].

The GJO site is on an approximately 7 m thick unit of riverbed sands and gravels in a sedimentary point bar formation that formed on bedrock (Figure 1 inset) along the Gunnison River [1]. The water table depth is controlled by the river stage with groundwater flowing into the point bar at the high river stage and out of the point bar at lower river stages, resulting in local groundwater flow directions changing up to 180 degrees [10]. A

water table depth of 2.7 m below ground surface at well 8-4S (Figure 1) is typical of water levels throughout most of the year, except at high river stages that occur mainly during nearby mountain snow melt in the spring and early summer. Ground surface elevations across the site are relatively similar and generally vary by less than 1 m, except for a higher elevation flood control dike along the perimeter.

Given the extreme changes in groundwater flow directions (generally -90 to $+90$ degrees from north) and the spotty nature of tailings deposition in low spots [10], the GJO site does not have a traditional contaminant plume with a single source zone and down-gradient groundwater contamination. Groundwater ultimately does discharge to the river, where uranium concentrations are highly diluted, but it can show measurable increases during low river flow at concentrations that generally remain near or below applicable surface water standards of 0.03 milligrams per liter (mg/L) [15]. Groundwater uranium concentrations are quite variable depending on river stage. The uranium concentration at well 8-4S (Figure 1) ranged from 0.097 to 0.73 mg/L from 2001 to 2020.

3. Materials and Methods

3.1. Fission-Track Radiography and Microscope Work

Fission-track radiography is done by placing mica over a standard thin section, irradiating the thin section and mica in a nuclear research reactor, and then examining, under a microscope (Zeiss model 472190-000/11), the fission tracks created in the mica from the radioactive decay produced by the irradiated uranium within the thin section. Areas with a higher density of fission tracks correspond to areas with more fission events and a higher concentration of uranium. Standard petrographic techniques were used to examine the fission tracks and thin sections with a microscope under plain light, reflected light, and crossed Nicols prisms. This methodology is summarized in [1], and a step-by-step guide is provided in Supplemental Data S1. S1 includes information on how to match and align the fission-track images with the thin section petrographic images, using small drill holes in the mica and thin section, which were created for this purpose. Once aligned, the fission-tracked mica and the original thin section are scanned using a high-resolution scanner (Epson Perfection V800 Photo) to create a “map” of each, which is an important step for locating individual mineral grains and being able to return to those grains later. The main advantage of using fission-track radiography is detecting the location of uranium in thin sections with very low bulk uranium concentrations (<15 mg/kg).

Cameras mounted on the microscopes were used to capture images of the fission-tracked mica and the thin sections. These two images were overlaid in a computer graphics program (Microsoft PowerPoint), where the transparency of the fission-tracked mica could be changed to compare with the corresponding thin section image. This allowed for images of where high solid-phase uranium concentrations occur (more fission tracks), which was used to guide efficient use of SEM-EDS techniques.

3.2. SEM-EDS Analyses

SEM-EDS microanalysis was completed after carbon-coating the irradiated, polished thin sections on an FEI Quanta 450 FEG scanning electron microscope at the U.S. Geological Survey Microbeam Lab in Lakewood, Colorado. After carbon coating, samples were handled and loaded into the vacuum chamber using gloved hands. High vacuum mode voltage varied from about 10 to 20 kilovolt, the beam current was about 1 nanoamp, and the working distance was about 11 mm, although these parameters varied depending on the sample. EDS spectra were acquired and initially identified through EDS acquisition software, with additional element interpretation through consultation with laboratory staff.

Typically, a backscattered electron (BSE) image of a sample would be used to find heavy minerals (such as uranium minerals) that show up in a brighter white, with successive magnification as needed. This technique can lead to a “hunt and peck” approach in new samples to find these uranium minerals. For samples with low uranium concentrations or highly disbursed uranium, the BSE approach may not detect any uranium, and

bright locations can often be other heavy elements (such as Fe, Ti, and Zr). The use of the fission-track radiography images avoids this approach, as the locations of elevated uranium (minerals or sorbed uranium) are already known from the fission-tracked images. With the SEM, a full thin section BSE map is created and then compared to the prior fission-tracked mica and plain light thin section images. The relative location of an area of interest, along with visual pattern matching of individual grains, allows for efficient “navigation” on the SEM to identify a specific spot. Details on these procedures are provided in Supplemental Data S1.

After finding a specific thin section area of interest provided by the fission-track radiography, the location is imaged again with the BSE approach, and specific spots can be analyzed with the EDS capabilities on the SEM. Element identification used the auto element identification feature of the Oxford Instruments, Aztec software. Since epoxy was used in the thin section creation, and it is high in carbon, carbon was suppressed in the elemental weight percent table for each spectrum, albeit carbon is still indicated in the spectrum. The other elemental weight percent values listed for each spectrum are for informational purposes only and are not considered quantitative. An interpretation as to the mineral phases is based on the relative intensity of the peak heights and comparison to spectra found in [16]. To later return to any specific area of interest, the location needs to be identified on the (1) fission-track mica image, (2) thin section, plain light image, or (3) full thin section BSE map—and preferably on all three.

4. Prior Solid-Phase Data

Prior work at the GJO site measured solid-phase uranium with four extraction techniques from multiple depths at 23 core locations [1] in an area near or below former tailings piles (Figure 1). Since detailed solid-phase uranium associations could not be identified with selective extractions (e.g., exact sorbing material such as clays or iron oxide), fission-track radiography and petrographic analyses were completed to assist in the identification of solid-phase uranium associations [1]. The solid-phase data, fission-track radiography, and microscopic analyses from [1] are summarized below, along with the initial conceptual model of the how uranium in the solid phase at the GJO site occurs. This work highlights the data gaps that led to the SEM-EDS work.

Samples from the intervals with the highest solid-phase uranium concentrations were collected for fission-track radiography and microscopic analyses from various depths at core locations GJAST-14, GJAST-15, GJAST-19, and GJAST-20 (Figure 1; Table S1). Solid-phase uranium concentrations with depth from GJAST-19 are similar to GJAST-14; thus, GJAST-19 is not discussed further. However, fission-track radiography, microscopic analyses, and SEM-EDS work for GJAST-19 are included in Supplemental Data S2 as a data release.

Figure 2 provides a summary of uranium concentrations in sediment collected from GJAST-14, -15, and -20 determined by (1) total digestion and (2) 5% nitric acid extraction (method details are provided in [1]). Five percent nitric acid extraction concentrations are considered indicative of total potentially mobile uranium (i.e., soluble uranium), and total digestion measures all uranium in the sediment [1]. Some of the highest concentration samples (GJAST-14-7, -8, and -9; GJAST-15-13; and GJAST-20-9, -10, and -11; see Figure 2) were the focus of the fission-track radiography and subsequent SEM-EDS work. The water table drawn in Figure 2 is based on measurements in nearby well 8-4S (Figure 1), which is strongly controlled by river stage. The 8-4S water level range plotted in Figure 2 does not include water levels influenced by high river stages that occur during spring snow melt.

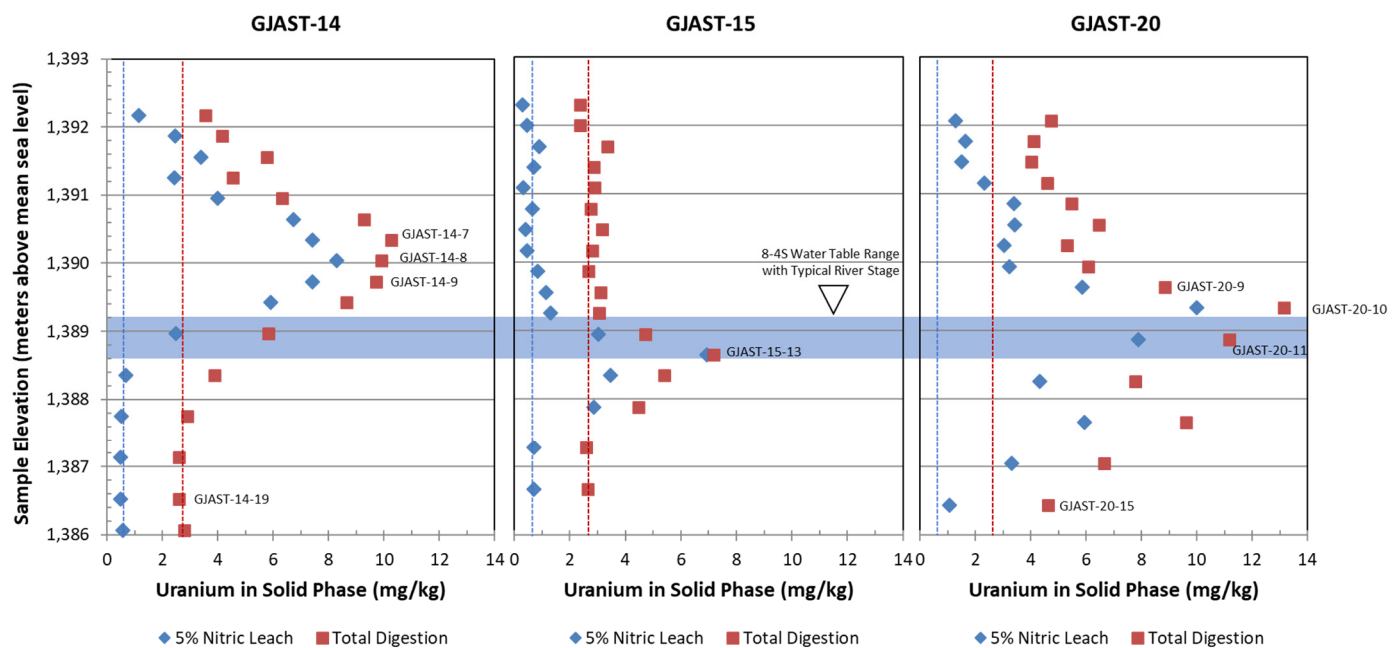


Figure 2. GJAST-14, 15, and 20 (locations in Figure 1) uranium concentrations with depth (National Geodetic Vertical Datum of 1929) for total digestion and 5% nitric acid extraction. Background values from GJAST-03 are 0.62 mg/kg for 5% nitric acid extraction (dashed blue vertical line) and 2.7 mg/kg for total digestion (dashed red vertical line). Individual identification labels indicate samples with fission-track radiography, thin section plain light microscopy, and SEM-EDS analyses. The first sample for all three locations is always 0.3 m (1 foot) below ground surface. The water level during typical stream flow conditions in nearby well 8-4S (Figure 1) is indicated as a range by the wide blue horizontal line, which does not include times when this well is influenced by high river stage and the water table rises substantially.

Data from GJAST-03 (Figure 1 [1]) provide background concentrations for uranium of 2.7 mg/kg for uranium total digestion and 0.62 mg/kg for 5% nitric acid uranium extraction (both plotted with vertical lines in Figure 2). GJAST-03 was close to the edge of the tailings, but it has concentrations similar to other single depth solid-phase uranium concentrations that are offsite [1]. Thus, GJAST-03 provides the best multidepth average concentration for this work. With these background concentrations, it is apparent that GJAST-14 does not typically have elevated uranium concentrations below the water table. GJAST-15 has elevated uranium concentrations at and just below the water table, and in GJAST-20, all samples are above background with highest concentrations at and just below the water table.

Other solid-phase information includes visual core logging [1]. Core logging estimated fill material depths (silt material), which included the first two samples at GJAST-14 and -15, and the first four samples in GJAST-20. However, fill material was difficult to distinguish from native silt, as the fill was a similar silt material collected locally. Native silt in GJAST-14 had some mottling in color in the unsaturated zone (possible evaporites) and darker colored, possible organic-related material with a sulfur smell was identified in GJAST-15 at the depths with the higher uranium concentrations.

In addition, column tests for GJAST-20 showed a release of calcium and sulfate at constant concentrations that were attributed to gypsum dissolution [1]. XRD analysis on the highest uranium concentration sample in GJAST-20 (GJAST 20-10, Figure 2) did confirm 6.5 wt % gypsum and 0.86 wt % calcite. Despite the higher concentrations of solid-phase uranium in this sample, no uranium minerals were detected with the XRD analyses. Gypsum at GJAST-20 is likely the result of low-pH, high sulfate waters being buffered by calcite dissolution, as would occur below sulfidic tailings. Institutional knowledge from site personnel who were present during the mill operation indicated that the GJAST-20 location was near a sump where hydrofluoric acid and other lab wastes were disposed.

Similar to the tailings reactions, hydrofluoric acid could produce gypsum precipitation upon buffering if enough sulfate was available.

5. Fission-Track Radiography and Microscopic Work

All resulting fission-track and thin section images are provided in Supplemental Data S2. For GJAST-14, Figure 3 shows dispersed fission tracks, with some uranium-rich grains having higher fission-track density (blue arrows in Figure 3). A bubble within the thin section shows that the mica itself does not produce any fission tracks (Figure 3).

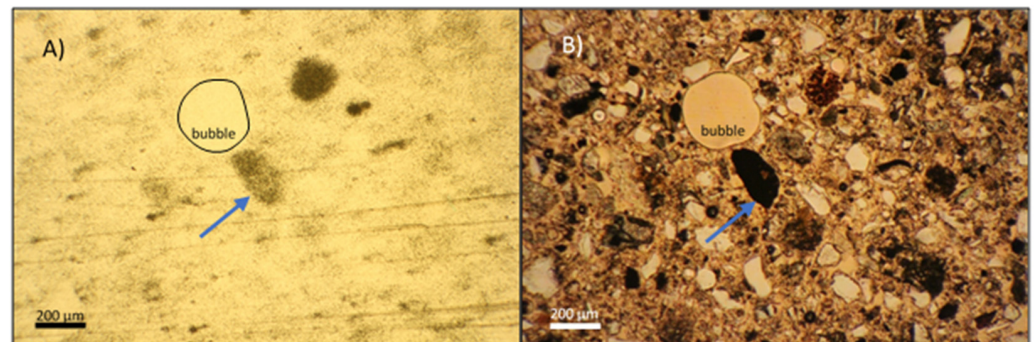


Figure 3. Images from sample GJAST-14-8 (Figure 2). (A) Fission-track image at $2.5\times$ magnification. (B) Thin section image in plain light at $2.5\times$ magnification. Blue arrows indicate a grain with inherent uranium.

For GJAST-15, Figure 4 shows the identification of a needle-like shape with a greater density of fission tracks. This needle-like shape was identified as organic material by seeing the cell structure in reflected light (Figure 4C). Another area with more fission tracks (see the red arrow in Figure 4A,B) could not be similarly identified in reflected light, as no cell structure was apparent.

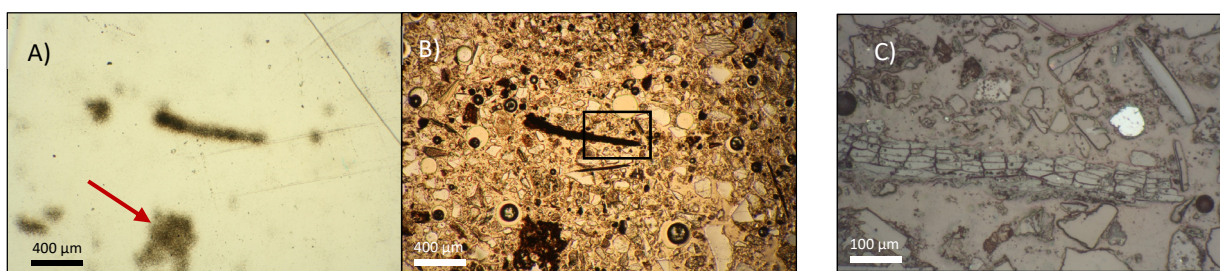


Figure 4. Fission-track and microscope images of sample GJAST-15-13 (Figure 2). (A) Fission track image at $2.5\times$ magnification. (B) Thin section in plain light of the same area at $2.5\times$ magnification. (C) Thin section in reflected light at $10\times$ magnification at the box located in (B) showing cell structure. Red arrow points to a high fission track particle where the cell/mineral structure could not be identified.

For GJAST-20, Figure 5 shows a high fission-track density (Figure 5A) associated with a mineral grain coating (Figure 5B). Figure 6 shows multiple grains with a high fission-track density in the cementing material between the grains. Due to the fine-grained nature of the coating and cementing materials, the actual mineralogy of these materials could not be identified using standard optical microscopy [1].

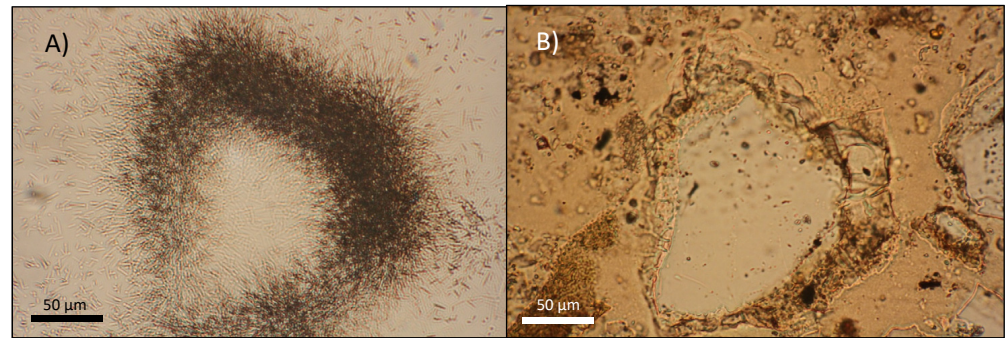


Figure 5. Fission-track and microscope images of sample GJAST-20-10 (Figure 2) with high fission-track grain coating. (A) Fission track image at $2.5\times$ magnification. (B) Thin section in plain light at $2.5\times$ magnification.

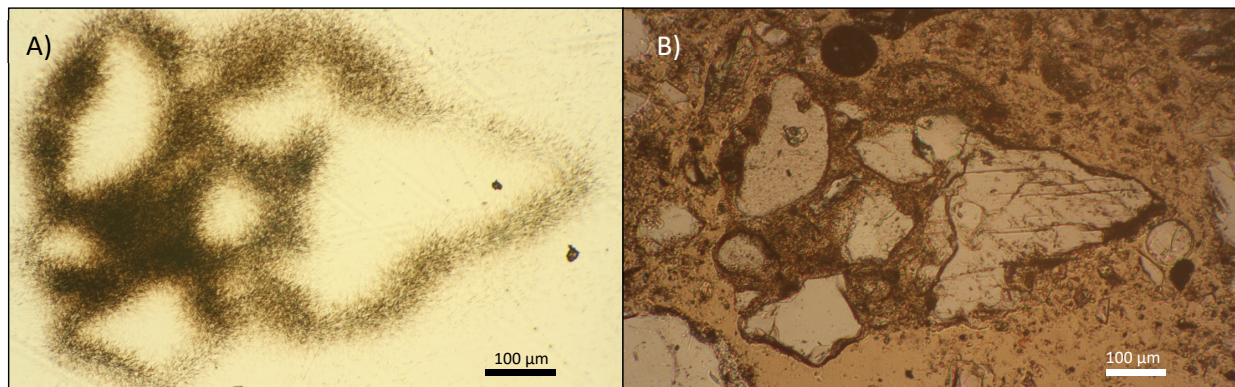


Figure 6. Fission-track and microscope images of sample GJAST-20-10 (Figure 2) with high fission-track cementing material. (A) Fission-track image at $10\times$ magnification. (B) Thin section in plain light at $8\times$ magnification.

In all samples, uranium inherent to mineral grains were identified. Figure 7 shows a grain for GJAST-20 with inherently high uranium concentrations. In Figure 7, the red colored mineral grain (later identified as pyroxene in the SEM-EDS work) is part of a larger rock fragment, but only the red mineral shows the high fission-track density. This demonstrates the sensitivity of the fission-track radiography to identify distinct locations within each thin section with elevated uranium concentrations, even when the overall total uranium content is low, in this case, 13 mg/kg.



Figure 7. Fission-track and microscope images of a portion of sample GJAST-20-10 (Figure 2) at $10\times$ magnification with high fission-track density in a distinct mineral grain. (A) Fission-track image. (B) The same portion of the thin section in plain light. (C) In crossed Nicols prisms.

6. Potential Solid-Phase Uranium Associations

Based on the fission-track images and thin section microscopy above, the three coring locations, GJAST-14, GJAST-15, and GJAST-20, have very different uranium mineralogy. Associations of uranium with the solid-phase mineralogy are as follows:

1. GJAST-14 appears to have elevated uranium dispersed throughout the sample (Figure 3), which is speculatively formed as evapotranspiration wicks and then deposits uranium from the underlying uranium-rich groundwater. This mechanism has been observed at other LM sites [13], but the exact mineralogy, such as sorption to clays, sorption to organics, incorporation into evaporite minerals, or uranium mineral precipitation cannot be identified with fission-track radiography and thin section microscopy alone. In addition, given the location of GJAST-14 (Figure 1), the original uranium deposition associated with the flow of tailings pore water into the underlying unsaturated zone is also a possibility.
2. The association of elevated uranium in GJAST-15 with high organic sediments preserved below the water table seems likely (Figure 4), but the confirmation of individual particles or grains being carbon rich is sometimes difficult to determine with standard microscopy.
3. For GJAST-20, the association of uranium with mineral coatings and cements is relatively clear (Figures 5 and 6), but the mineralogy of these coatings and cements cannot be identified with standard microscopy because of the extremely fine-grained and sometimes amorphous nature of these materials.

The original method of combining fission track radiography with traditional optical microscopy is inadequate for understanding the mineral phases with associated uranium in the study area. The subsequent sections discuss the methods and results of combining the fission-track radiography with SEM-EDS techniques to enhance understandings of solid-phase uranium associations at the GJO site.

7. SEM-EDS Results and Discussion

All the images for each thin section and fission-tracked mica are provided in Supplemental Data S2. Each folder in S2 has sample identification numbers that correspond to those provided in Figure 2 and Table S1. Within each folder, one file (thin section_fission tracks GJ **-*.pptx) includes all the fission-track mica and thin section images for that sample. The first page in these files has the full-sized thin section image with an overlaid fission-track mica image. Locations of interest are numbered, and subsequent pages are fission-track mica and thin section plain light overlays in the order of the numbered locations. All fission-track mica images can be changed in transparency to compare with the underlying thin section image. In S2, all fission-track mica images have been initially set to a 25% transparency level for easy initial viewing. For the SEM-EDS work, a BSE image map of the full thin section was completed, but it was not included in S2, since the fission track/thin section overlay images already locate areas of interest for examination under high magnification.

Additional files in S2 include SEM-EDS images and spectrums with numbering to match the locations of interest for each thin section (GJO Sediment_**-*.location#.pdf) along with a summary file of notes taken while at the SEM (**-*.SEM NOTES and SUMMARY.pdf) with petrographer George Breit (U.S. Geological Survey (USGS) emeritus geologist). A final file (thin section_fission tracks GJ **-*.pptx) has the SEM-BSE images of all locations of interest pasted into the original fission track/thin section overlay images file. This final file has interpretations added directly to the images. The following discussion uses key images from S2 to highlight interpreted uranium associations for key samples from GJAST-14, GJAST-15, and GJAST-20.

7.1. Fission-Track Image Maps

Figures 8–10 are the fission-track mica images for GJAST-14-8, GJAST-15-13, and GJAST-20-10, respectively (Figure 2), with the location of zoomed-in areas of interest for subsequent figures. The fission-track mica image from the deepest sampling at GJAST-14, GJAST-14-19 (Figure 11) is provided for comparison, as the solid-phase uranium concentration in this sample is close to background (Figure 2) and is representative of solid-phase concentrations within the uranium contaminated groundwater. GJAST-14-19 (Figure 11) has fewer fission tracks, as expected, with its lower uranium concentration. Overall, these figures show that the density of fission tracks on the mica images do not clearly relate to quantitative solid-phase uranium concentrations. In addition, for GJAST-14-8 (Figure 8 and S2), a subtle distribution of fission-track shading can be seen throughout the image. This is highlighted with the locations of bubbles within the thin section that have no fission tracking (Figure 8), but it is better viewed by changing the fission-track overlay transparency using the files in S2. GJAST-15-13 has more discrete fission-tracked particles (Figure 9), and GJAST-20-10 is the only location where fission tracks are associated with grain coatings (see arrow in Figure 10, but it is better viewed in S2).

7.2. Fission-Track and Thin Section Images with Addition of SEM-EDS

For each core location—GJAST-14, GJAST-15, and GJAST-20—the following discussion includes fission track, thin section plain light, and SEM-BSE images zoomed in to the areas of interest shown in Figures 8–10. SEM-EDS spectrums are included to highlight the mineralogy. All samples have inherent uranium associated with mineral grains that is likely not mobilized into groundwater under normal conditions and accounts for the total digestion of uranium being higher than the 5% nitric acid extraction for uranium by about 2 mg/kg (Figure 2). This inherent uranium was seen in all of the SEM work (S2). Since the focus of this work was to identify mineralogical associations of the mobile uranium, only one inherent uranium image is provided (GJAST-14-8 area 5, Figure 8, discussed below).

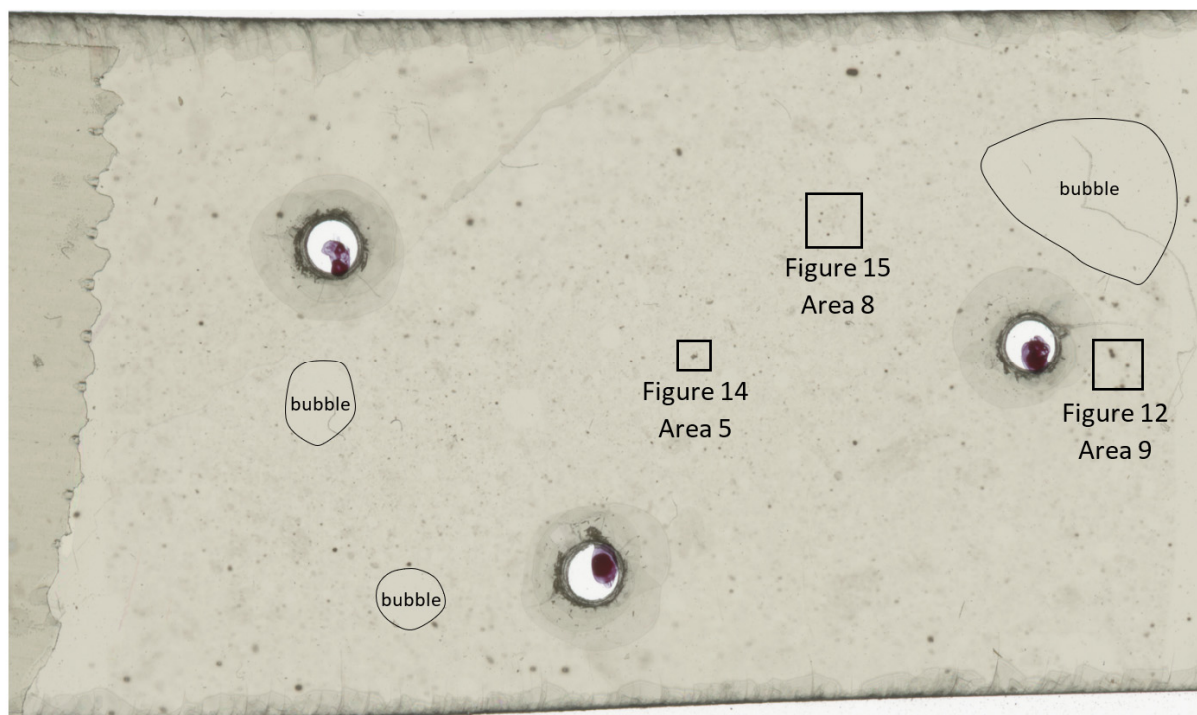


Figure 8. Fission-track mica image for GJAST-14-8 (total digestion uranium concentration of 9.92 mg/kg). Squares indicate zoomed-in areas with associated figure numbers. White circles are drill holes used to align the fission-tracked mica and the thin section. Length is 38 mm.

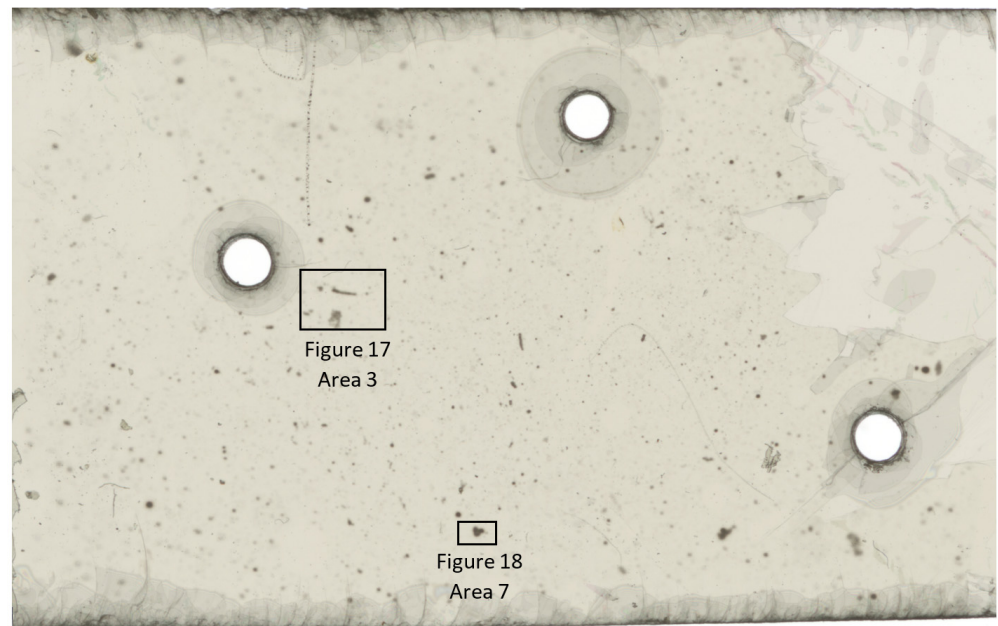


Figure 9. Fission-track mica image for GJAST-15-13 (total digestion uranium concentration of 7.18 mg/kg). Rectangles indicate zoomed-in areas with associated figure numbers. White circles are drill holes used to align the fission-tracked mica and the thin section. Length is 32 mm.

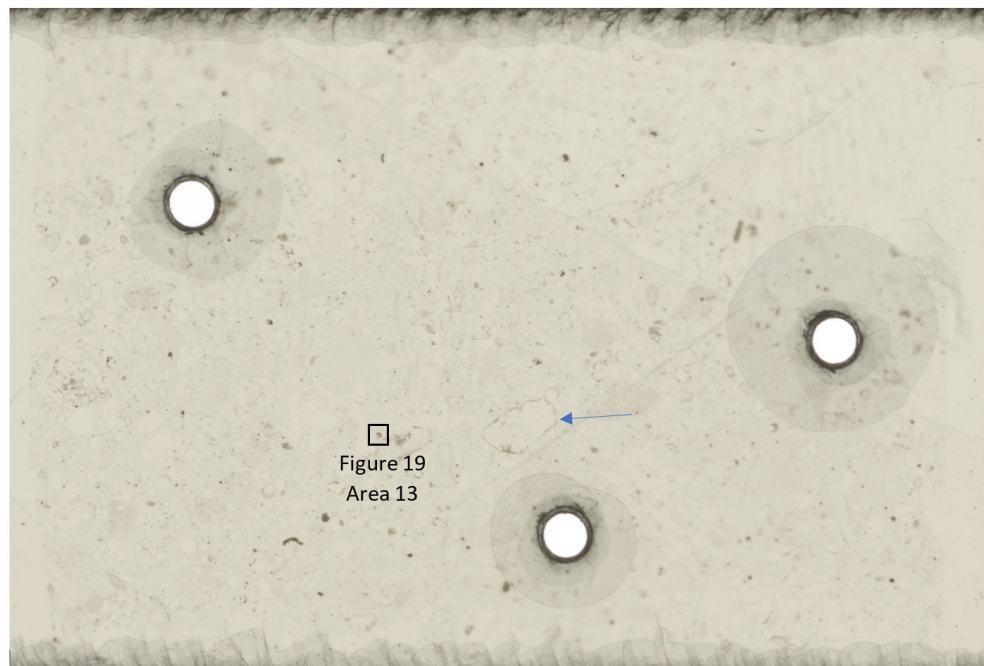


Figure 10. Fission-track mica image for GJAST-20-10 (total digestion uranium concentration of 13.2 mg/kg). Arrow indicates large grain with a fission-track rind. Rectangle indicates zoomed-in area with associated figure number. White circles are drill holes used to align the fission-tracked mica and the thin section. Length is 32 mm.



Figure 11. Fission-track mica image of GJAST-14-19 (total digestion uranium concentration of 2.60 mg/kg). Shown as a background comparison. White circles are drill holes used to align the fission-tracked mica and the thin section. Length is 40 mm.

7.2.1. GJAST-14

For GJAST-14-7, GJAST-8, and GJAST-9 (highest uranium concentrations in GJAST-14, Figure 2), distinct grains with higher fission-track density appear to be pieces of organic carbon in addition to grains with inherent uranium. This organic carbon can be found in distinct pieces with cell structures (S2) or in a more amorphous form, as seen in the SEM-BSE images (Figure 12). As a result of the amorphous nature of the carbon, epoxy often occurs in the middle of the carbon structure, but this epoxy contains Cl in addition to carbon, so it is easy to identify (spectrum 649, Figures 12 and 13). Higher carbon rinds/rims were lower in Cl (spectrums 648 and 650, Figures 12 and 13), allowing for the identification of these areas as being mainly carbon, along with the visual identification from the BSE image (Figure 12). The carbon with elevated uranium in GJAST-14-7, GJAST-8, and GJAST-9 has variable amounts of Ca, Mg, Na, S, Fe, Al, and Si (S2 and Figure 13, spectrums 648 and 650) and occasional measurable uranium. However, uranium is usually considered below the SEM-EDS detection limits (elements in red, Figure 13). Some of this elemental variability may be associated with minerals deposited during the evaporation of contaminated groundwater or tailings fluids, such as calcite, gypsum, and sodium sulfate salts. However, no distinct evaporite minerals were identified, and such minerals may have been dissolved and dispersed during the thin sections cutting process. The thin sections for this work were cut using a water-cooled blade. Future work should use an oil-cooled blade to avoid potential dissolution.

The unique mineralogy in GJAST-14-8 includes a pyrite framboid (now oxidized) next to a piece of carbon (Figure 12). The EDS spectrum identified this pyrite framboid as being oxidized, as the elemental composition was mainly iron and oxygen (spectrum 660, Figure 13). It is difficult to determine if the fission-track image correlates with higher uranium on this iron oxide framboid, as it is very close to the fission tracking from the organic carbon that visually dominates this portion of the image (Figure 12). This pyrite to iron oxide conversion is consistent with this sample being above the typical water table but being within a zone that can convert from reducing to oxidizing conditions with a

transiently high water table controlled by the river. These transiently reduced zones have been documented at other LM sites [17].

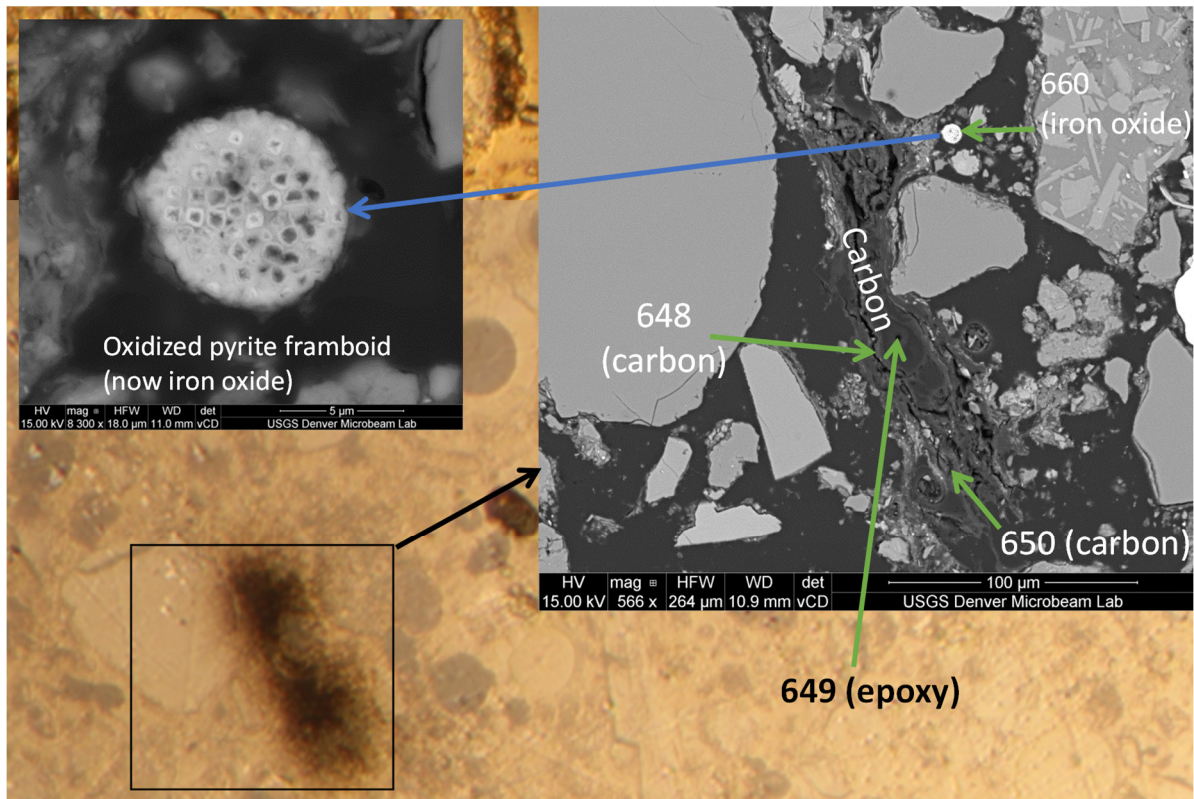


Figure 12. GJAST-14-8 area 9 (Figure 8), thin section plain light background with fission-track overlay at 25% transparency with added SEM-BSE images. Numbering corresponds to spectrums in Figure 13.

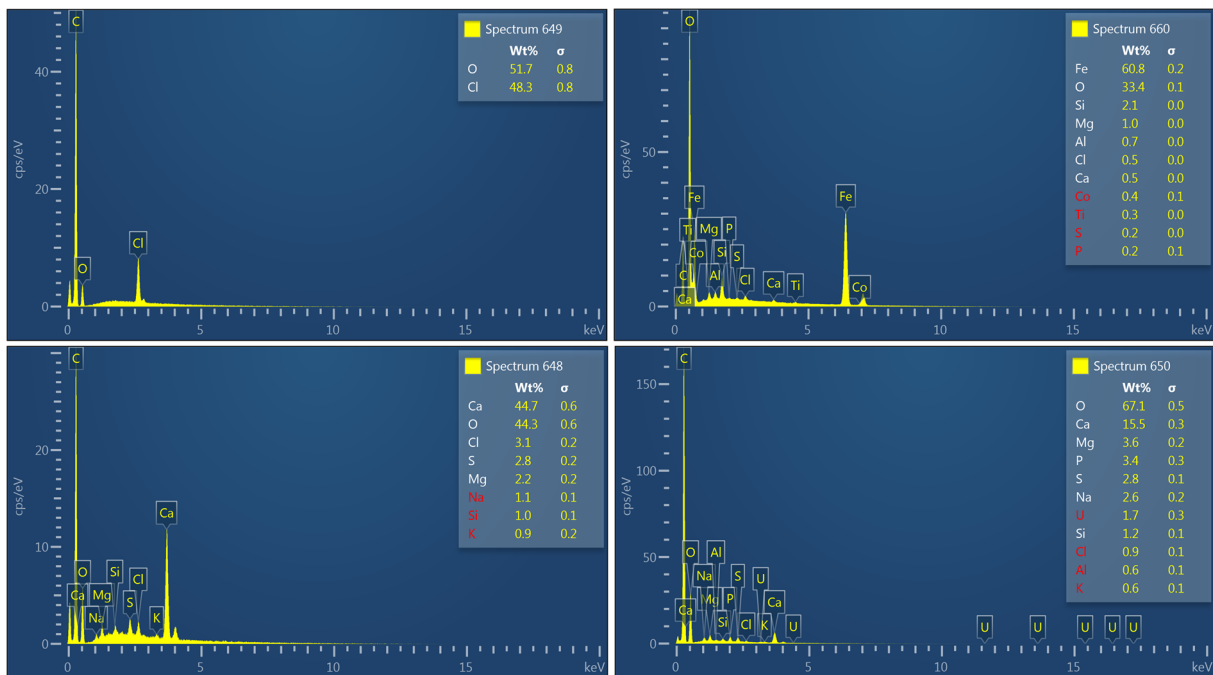


Figure 13. SEM-EDS spectrums at locations in Figure 12. Elements in red are below the SEM-EDS detection limit.

Additional distinct locations of high fission-track density at GJAST-14 include uranium inherent in mineral grains. An example of this is a titanium oxide grain associated with uranium fission tracking (Figure 14). The fission-track density is resolved enough to show the lack of uranium within the quartz that is part of the whole grain. Since the thin sectioning cut through this grain, the uranium is likely incorporated within the titanium oxide mineral structure. Uranium content is highlighted by the fission-track density, but the SEM-EDS identifies the mineral as being titanium oxide with uranium being below the EDS detection limit.

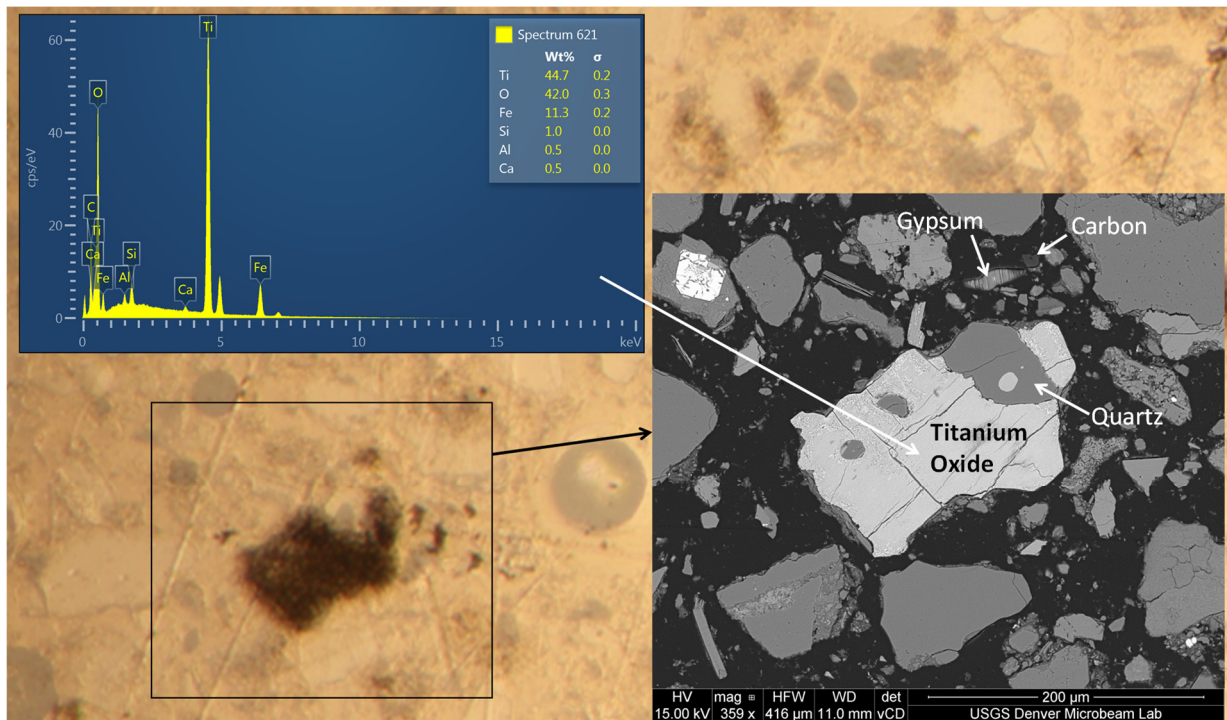


Figure 14. GJAST-14-8 area 5 (Figure 8), thin section plain light background with fission-track overlay at 25% transparency with added SEM-BSE image and titanium oxide EDS spectrum.

Other than the fission tracks associated with carbon and inherent uranium in mineral grains, the fission-track pattern for GJAST-14-7, GJAST-8, and GJAST-9 (S2, and Figure 8 for GJAST-14-8) is subtly associated with clay balls in the original samples that were preserved during epoxy impregnation and thin section creation. This association is difficult to show in print and is best seen by changing the transparency in the fission-track image overlaid on the thin section plain light image (S2). The “cloud” pattern in Figure 8 could not be resolved with any SEM-EDS work because no distinct area with high fission-track density could be resolved. However, area 8 in GJAST-14-8 (Figure 15 and S2) shows one of these clay balls with three locations of higher fission-track density. Two of these locations are related to carbon (Figure 15 and spectrum 634 in Figure 16), and one is elevated uranium associated with a zircon grain (Figure 15 and spectrum 635 in Figure 16). The matrix in this ball was confirmed as clay material (Figure 15 and spectrum 638 in Figure 16). Spectrum 644 in Figure 16 is included for a titanomagnetite grain that has a brighter color in the BSE image due to the presence of heavier elements (Fe and Ti), but it does not show a uranium fission-track signature (Figure 15).

SEM-EDS analyses on GJAST-14-19 (sand and gravel aquifer) were completed at only four locations. These analyses did indicate uranium inherent in mineral grains (titanomagnetite in area 2, feldspar grain in area 4, apatite grain in area 8, see S2), and one location with uranium associated with a carbon piece (area 2, see S2). Uranium associated with clays was not seen. These data are consistent with this location having a minor

amount of sorbed uranium from the groundwater (5% nitric acid extraction for uranium at 0.49 mg/kg) and the total digestion uranium having uranium inherent in mineral grains (2.60 mg/kg).

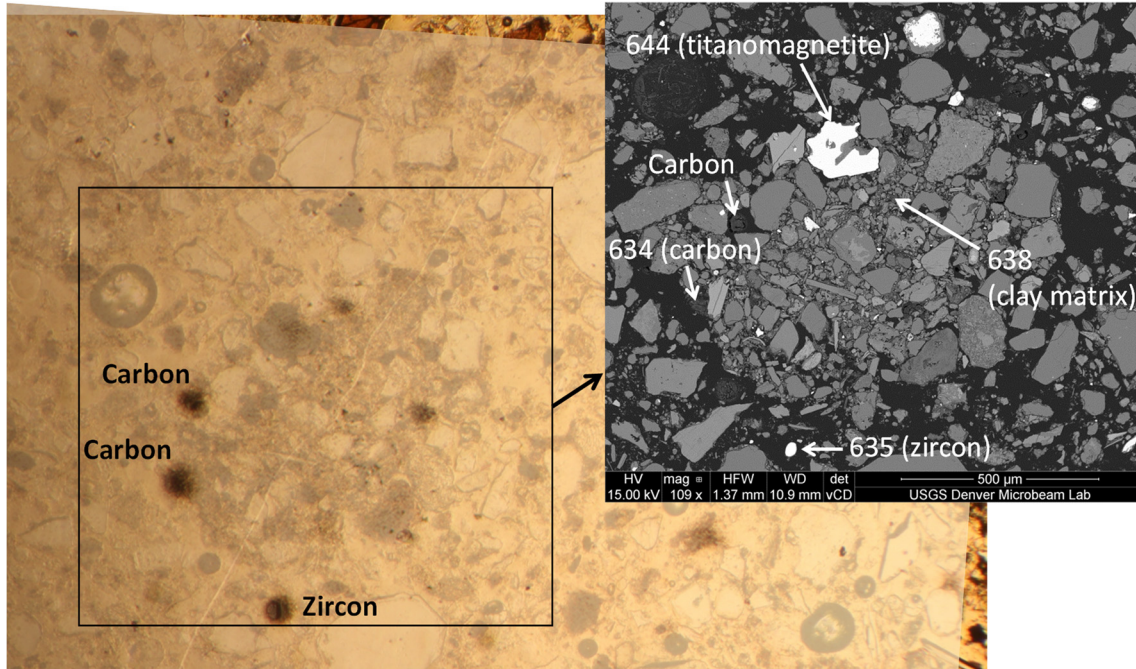


Figure 15. GJAST-14-8 area 8 (Figure 8), thin section plain light background with fission-track overlay at 25% transparency with added SEM-BSE image of clay ball with three high fission-track spots, two carbon pieces, and one zircon grain. Numbering corresponds to spectrums in Figure 16.

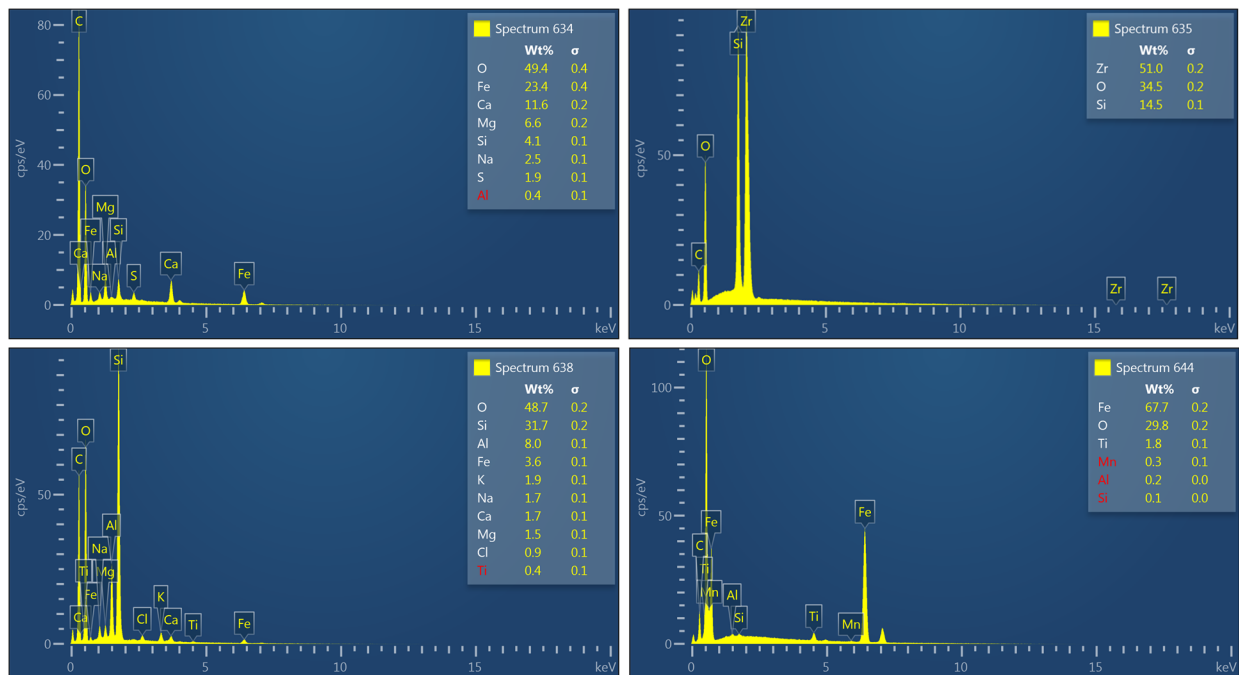


Figure 16. SEM-EDS spectrums that are indicated in Figure 15. Elements listed in red are below the SEM-EDS detection limit.

7.2.2. GJAST-15

For coring location GJAST-15, GJAST-15-13 (Figure 2) is the only sample with fission-track, thin section, and SEM-EDS analyses. Multiple areas of the thin section with higher fission-track density were examined (S2), and except for mineral grains with inherent uranium, these fission tracks are related to organic carbon. Results from GJAST-15-13 area 3 (Figure 9) show three locations where carbon is related to high fission-track density (Figure 17). The SEM-EDS spectrum for this carbon-rich material is similar to those from GJAST-14, GJAST-7, GJAST-8, and GJAST-9 (S2), but it tends to have a more consistent detection of Fe (similar to spectrum 407 in Figure 17). Compared to the prior image with just fission tracks and the thin section (Figure 4), the location with high fission tracks and an apparent cell structure is confirmed as an organic material with the SEM-EDS spectrum by the high organic content (spectrum 407, Figure 17). The bright spots in the SEM-BSE image are pyrite with minimal oxidation (spectrums 399 and 400 in S2). In addition, the location without a distinct cell structure (see the red arrow in Figure 4) is confirmed as high organic content (S2) but also with a clay matrix present (spectrum 422, Figure 17) within the amorphous organic material.

Unoxidized pyrite was also found in GJAST-15-13 in area 7 (Figure 9) as a distinct framboid (Figure 18) associated with a piece of organic carbon. In the upper right portion of this piece of organic carbon, slightly oxidized pyrite is present (spectrum 469), with a greater fission-track density. Overall, the pyrite in GJAST-15-13 is minimally oxidized compared to GJAST-14-7, GJAST-8, and GJAST-9, which corresponds with GJAST-15-13 being consistently below the water table (Figure 2), thus being protected from rapid oxidation as might occur in unsaturated sediments. In addition, the presence of barite (Figure 18) is a likely indicator of high sulfate concentrations in the past, as barite is sparingly soluble.

7.2.3. GJAST-20

Four samples at GJAST-20 have fission-track radiography and thin section plain light imaging: GJAST-20-9, GJAST-20-10, GJAST-20-11, and GJAST-20-15 (Figure 2) with total digestion uranium concentrations of 8.85, 13.2, 11.2, and 9.63 mg/kg, respectively (Table S1). SEM-EDS analyses were only completed on GJAST-20-9, GJAST-10, and GJAST-15 (S2). Fission tracks associated with these elevated uranium concentrations are visible in all GJAST-20 samples (S2), but GJAST-20-10 stands out as having fission tracks occurring as grain coatings (Figure 10).

Unique SEM-EDS attributes in GJAST-20-9 include area 3 with high fission tracking due to uranium associated with apatite but with an unusually high fluoride concentration (spectrums 706 through 710 in S2). Similarly, GJAST-20-9 area 9 had two areas of clay coatings that were high in fluoride (spectrums 732 and 733 in S2) but did not have a high fission-track density. These data seem to confirm the institutional knowledge that this coring location was close to a leaky sump where hydrofluoric acid was disposed. GJAST-20-9 area 13 was also unique with a very strong fission track signature (S2) due to a small inclusion of brannerite (UTi_2O_6 , see spectrum 747) within a degraded biotite grain (S2).

In GJAST-20-10, the higher density of fission tracks around grains (Figure 10) is associated with clays and a unique Al/Si gel. This Al/Si gel can be identified as not being clay due to its high Al content with a distinct lack of clay-related elements such as Mg and K (see spectrums 219 and 775 in Figures 19 and 20). In addition, the SEM-BSE images of the Al/Si gel have a “dried gel” appearance with distinct shrinkage cracks and a consistent color (Figures 19 and 20), compared to the more mottled appearance of the clays that occur between grains and the Al/Si gel that forms a rind around the mineral grain (Figure 20). This Al/Si gel was seen in the thin section plain light imaging (Figure 5) of the same grain shown in Figure 19 but could not be mineralogically identified, showing how SEM-EDS analysis adds information important to interpreting the uranium-enriched mineral phases in these samples. Trace amounts of Ca, S, Mg, Fe, As, and V consistently occur within the Al/Si gel structure (Figures 19 and 20, and S2). It appears likely that low-pH influent water, either tailings derived or from laboratory disposal wastes, dissolved the native

sediments, releasing Al and Si from aluminosilicates and providing elements for this “gel”. Although the constituents in these low-pH fluids were never measured, it likely included high concentrations of Al that precipitated during buffering reactions (i.e., native calcite dissolution), along with other pH-sensitive elements (such as Fe, As, and V). Such buffering reactions could also precipitate gypsum, as reflected in trace Ca and S concentrations in the EDS spectra (Figures 19 and 20), and from column testing [1], which may be within the Al/Si gel structure at a very fine scale. This very fine scale may be the reason no distinct gypsum mineral grains were identified with the SEM in any grain coatings. Cementing material in a duplicate sample of GJAST-20-10 with high fission-track density (Figure 6) is mainly clay with a small amount of Al/Si gel (Figure 20, the same grain as in Figure 6). In Figure 20, the Al/Si gel versus the higher clay content can be seen texturally in the SEM-BSE images. Some Fe is detected in the Al/Si gel and may also be derived from dissolved aluminosilicates in sediments (see above). Iron occurs in higher concentrations within the clays (Figures 19 and 20).

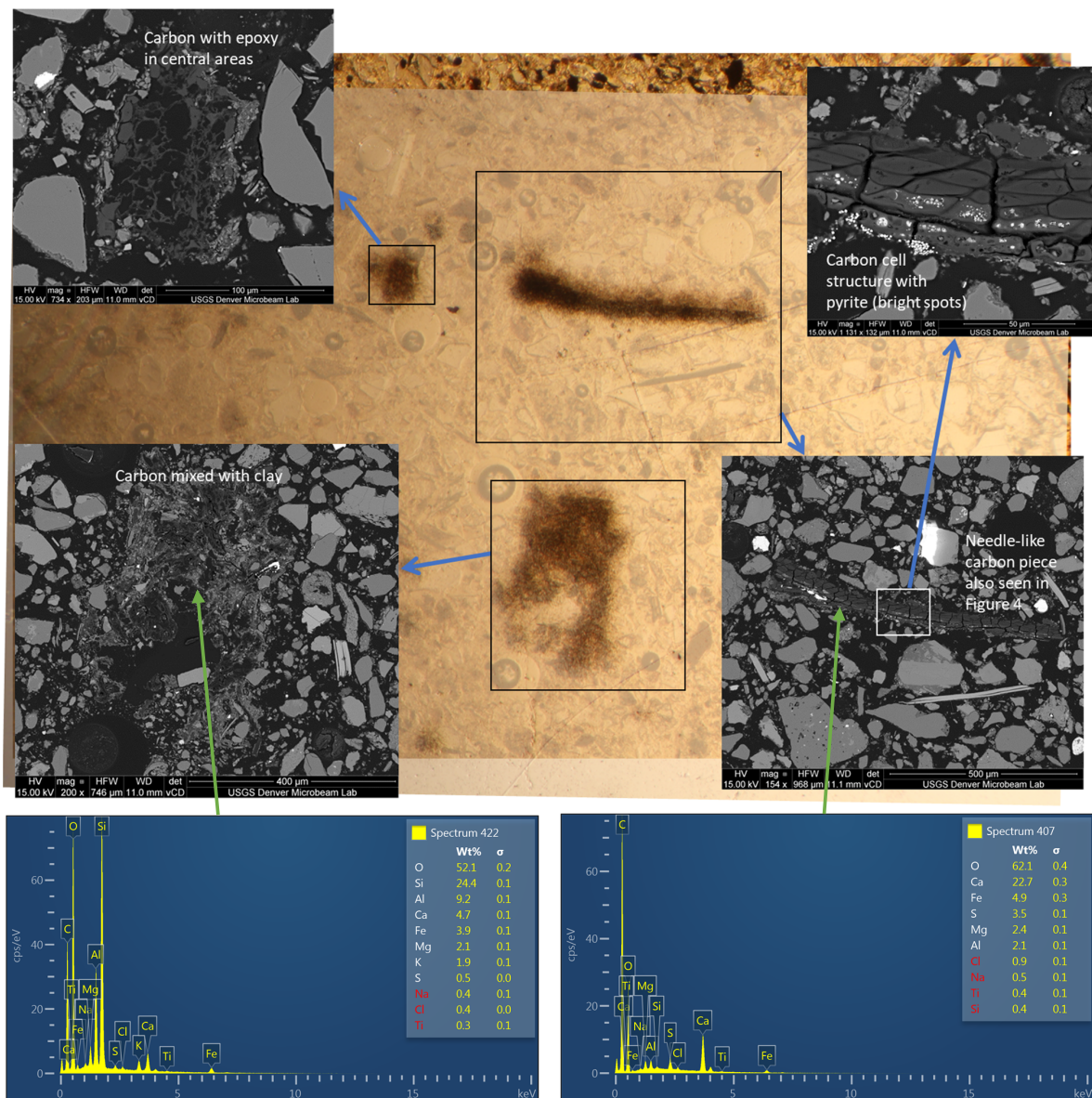


Figure 17. GJAST-15-13 area 3 (Figure 9), thin section plain light background with fission-track overlay at 25% transparency with SEM-BSE images.

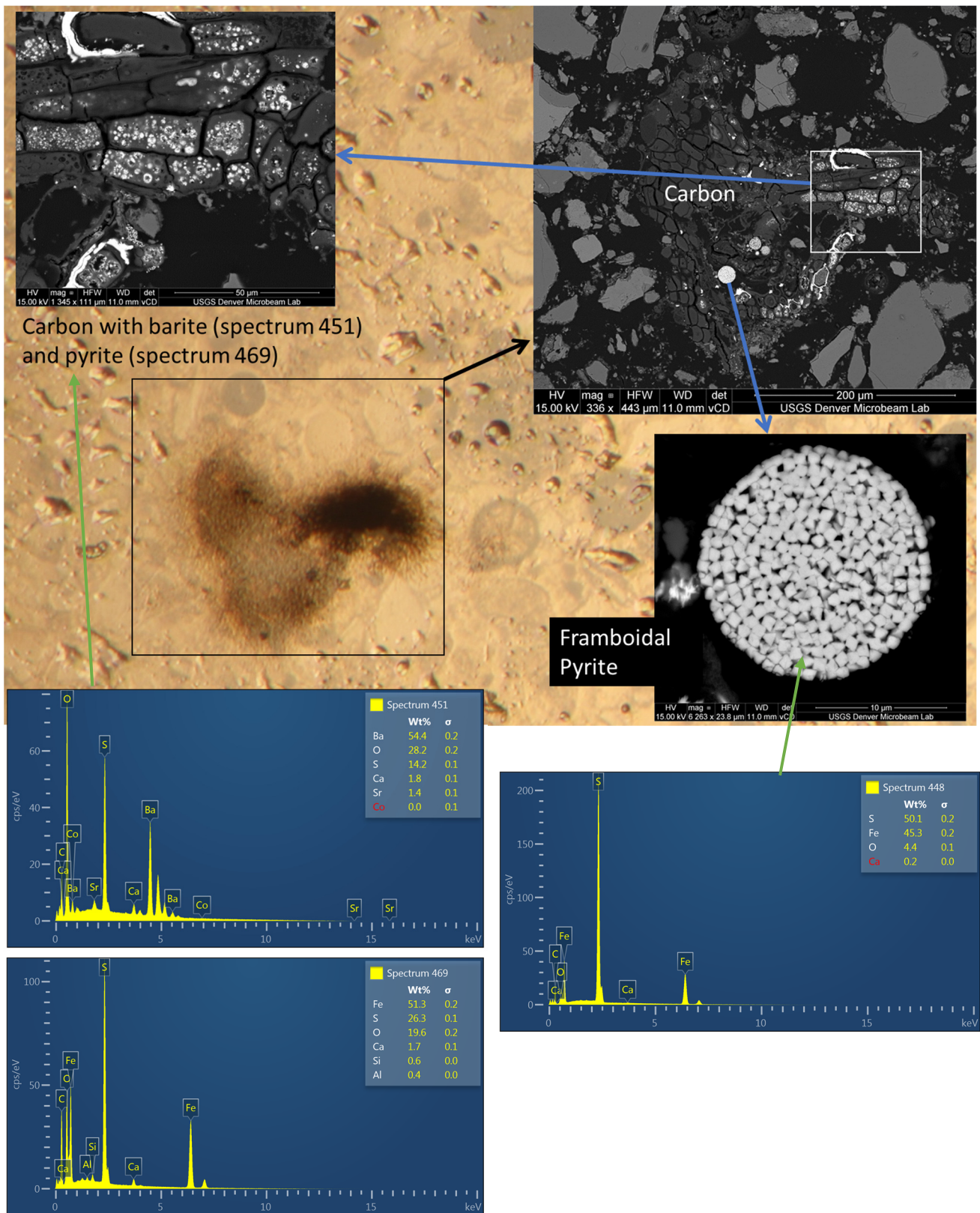


Figure 18. GJAST-15-13 area 7 (Figure 9), thin section plain light background with fission-track overlay at 25% transparency with added SEM-BSE images and EDS spectra. Bright white streaks are barite.

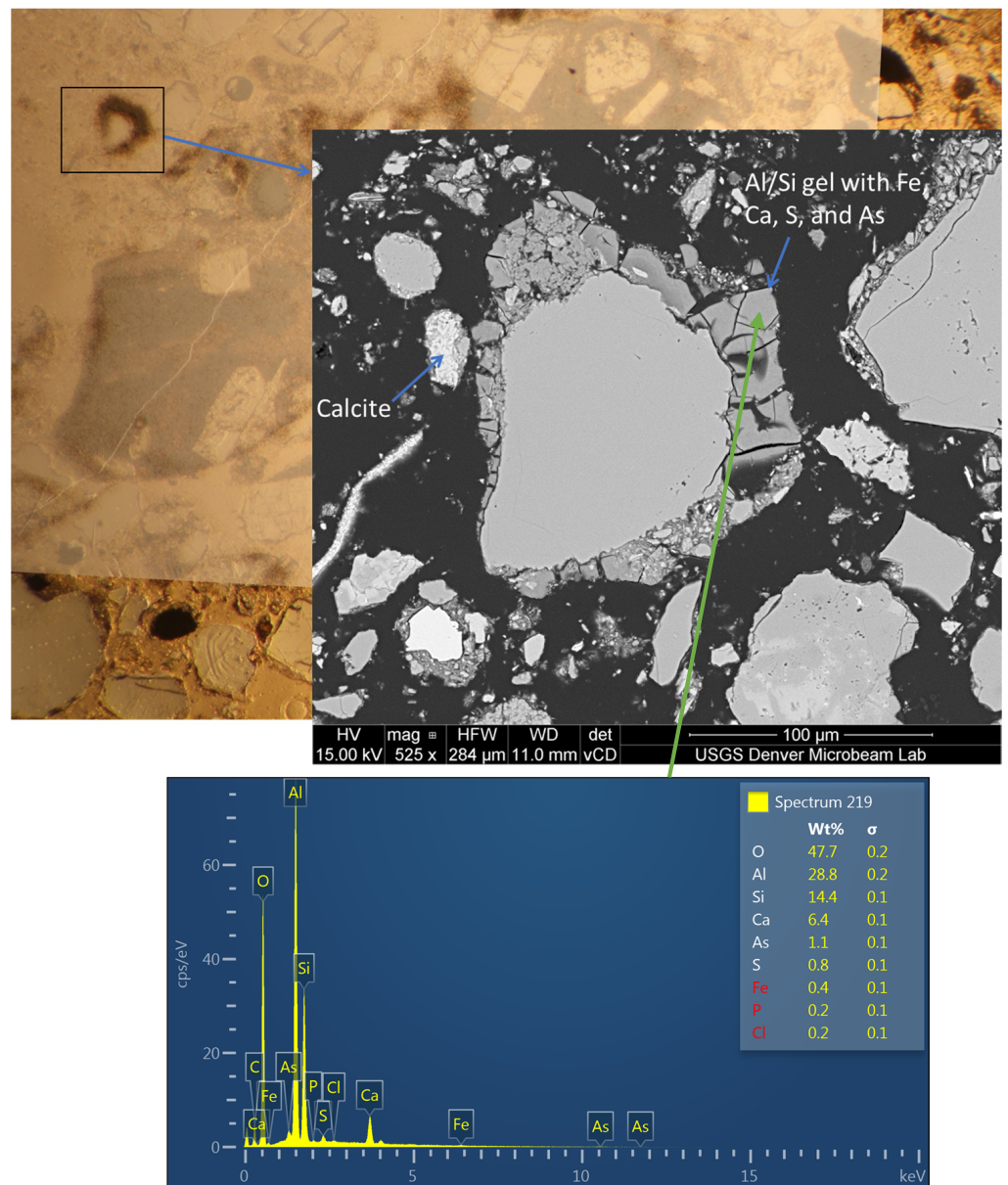


Figure 19. GJAST-20-10 area 13 (Figure 11), thin section plain light background with fission-track overlay at 25% transparency with added SEM-BSE and spectrum images.

In GJAST-20-15, area 6 also had an Al/Si gel (file “thin section_fission tracks GJ 20-15 with SEM.pptx” in S2) but with lower fission-track density than seen in GJAST-20-10. GJAST-20-15 had two locations with pieces of iron (maybe steel) that had associated uranium based on higher fission track density (see areas 4 and 8 in S2; same file as above). The sorption of uranium from the groundwater to these iron pieces is expected, but the source of this iron is unclear. The boring log for GJAST-20 indicates remedial excavation and backfilling to approximately 1.4 m compared to the 4.7 m depth for sample GJAST-20-15.

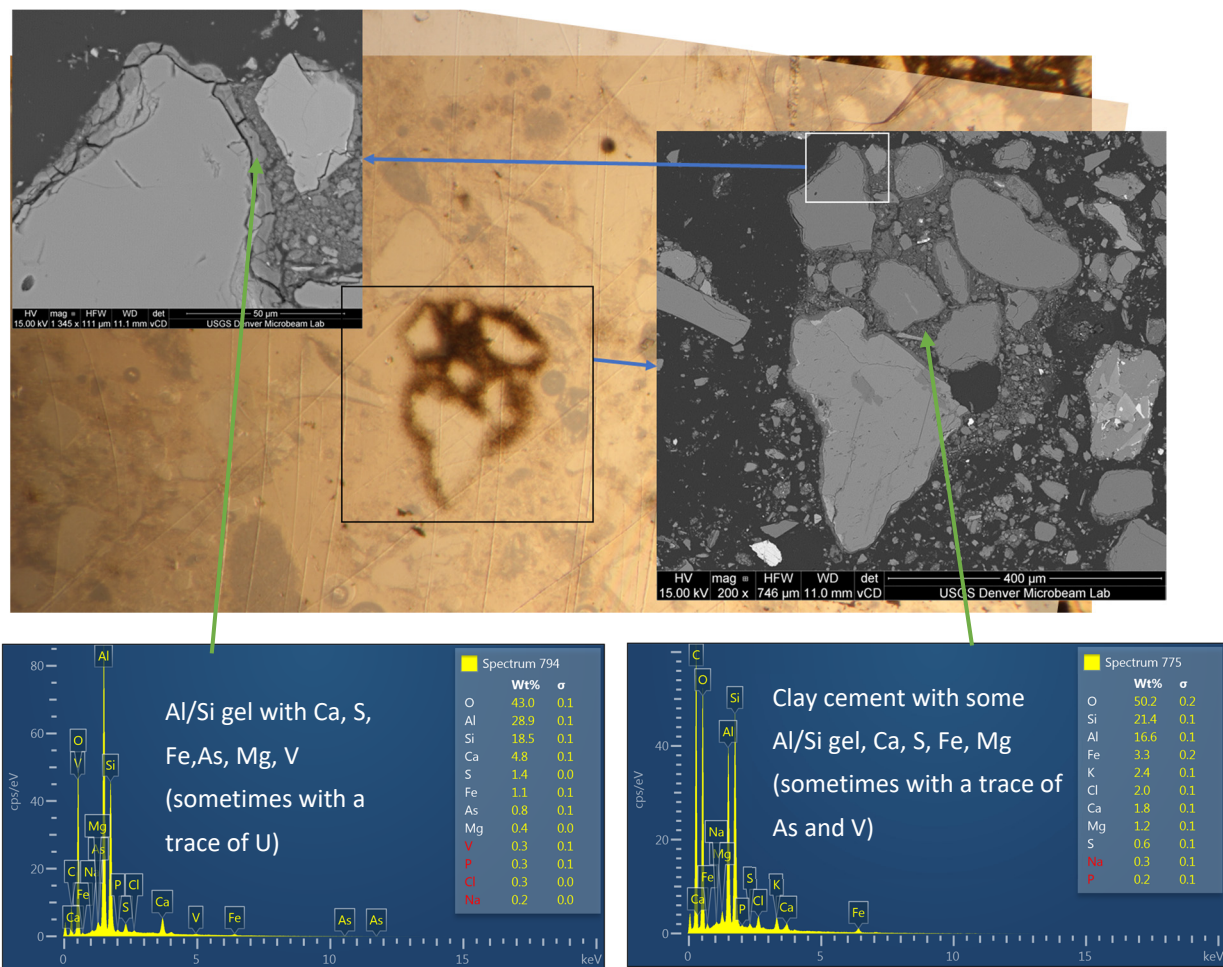


Figure 20. GJAST-20-10 duplicate area 1 (see S2), thin section plain light background with fission-track overlay at 25% transparency with SEM-BSE images.

8. Updated Solid-Phase Uranium Associations with SEM-EDS Information

Compared to uranium mineralogic associations from just fission-track images and thin section microscopy, the SEM-EDS analyses refine the uranium mineralogy for each coring location as follows:

- GJAST-14: The dispersed nature of fission tracks associated with evaporites cannot be conclusively confirmed but seems likely. SEM-EDS work clarifies that uranium is associated with carbon in the unsaturated zone and not with clays or iron oxides. Fission tracks associated with carbon that contain trace Ca, Mg, S, and Na, common in evaporite minerals, provide added evidence of a possible uranium/evaporite association. Uranium sourced from tailing-derived fluids that sorbed to the unsaturated zone carbon is still a possibility.
- GJAST-15: Uranium associated with organic carbon related to a sorption/desorption mechanism is confirmed.
- GJAST-20: SEM-EDS identified a precipitated Al/Si gel with elevated uranium concentrations based on associated fission tracks. This gel likely provides the source of calcium and sulfate in column effluent [1] along with trace metals such as uranium and vanadium. Distinct gypsum precipitation could not be confirmed, but it appears likely based on the presence of Ca and S within the Al/Si gel and the detection of gypsum in these samples using XRD. Elevated uranium is also associated with clay coatings and cements and suggests a uranium sorption/desorption process at this location related to the clays. The exact uranium processes related to the Al/Si gel,

such as sorption/desorption, dissolution, or a requirement of uranium dispersion through the gel coating to the groundwater is unknown.

9. Conclusions

The use of fission-track radiography coupled with SEM-EDS provides an efficient technique for identifying areas of a thin section with elevated uranium that would not be possible otherwise. For environmental samples with relatively low uranium concentrations, SEM-BSE images support the “bright spot” identification of uranium-enriched minerals on thin sections such as zircon and titanium oxide that are insoluble in groundwater. However, areas with low levels of elevated uranium in mineral phases that are soluble in groundwater cannot be detected with typical SEM-BSE analysis but require fission-track radiography. Fission-track radiography becomes a “guide map” for zooming in and investigating these areas with the SEM. Then, the use of EDS spectrum at these elevated uranium locations provides a means for identifying the associated mineralogy.

The SEM-EDS mineralogy associated with higher uranium content, as identified by the fission-track density, provides information on potential uranium mobility control mechanisms (e.g., sorption on clay and organics, immobile uranium in mineral grains, or incorporation in Al/Si precipitates). Thus, the initial mechanism for uranium mobility controls is tested and refined to provide useful information for guiding additional testing at the laboratory and field scales.

Supplementary Materials: The following are available online at <https://doi.org/10.5281/zenodo.4784267>, Supplemental Data S1: Detailed Fission-Track Radiography Methods, Table S1: Details for GJO Sediment Samples with Completed Thin Sections. Supplement Data S2: Fission-Track Radiography and SEM-EDS Images and Data Files, multiple folders.

Author Contributions: Conceptualization, R.H.J.; methodology, R.H.J., S.M.H., A.D.T.; formal analysis, R.H.J.; investigation, R.H.J., S.M.H., A.D.T.; resources, R.H.J., S.M.H.; writing—original draft preparation, R.H.J.; writing—review and editing, R.H.J.; visualization, R.H.J., S.M.H. and A.D.T.; supervision, R.H.J.; project administration, R.H.J. All authors have read and agreed to the published version of the manuscript.

Funding: Funding for this work was provided by the U.S. Department of Energy Office of Legacy Management through contract DE-LM0000421.

Data Availability Statement: The data presented in this study are contained within the article and in the supplementary materials.

Acknowledgments: Stan Morrison’s efforts in initiating the Plume Persistence Project under AS&T are greatly appreciated. His initial work with the identification and oversight of coring work, laboratory extractions, and preparation of initial samples for fission-track radiography work formed the foundation for this project. In addition, Stan’s microscope and camera set up made initial imaging possible. We also thank Bob Zielinski (USGS retired) for advancing the procedures for fission-track radiography and sharing his knowledge with us. His assistance and coordination with the USGS TRIGA Reactor in Denver, CO was invaluable. Thanks to Heather Lowers and the staff at the USGS Denver Microbeam Laboratory for supporting all aspects of the SEM-EDS work. George Breit (USGS retired) was a major contributor to the SEM-EDS analyses, and he was always there to help troubleshoot any issues with the thin section SEM imaging. In addition, he was our petrographer for identifying minerals with the SEM. His ability to look at EDS spectrums and immediately convert those to minerals is legendary.

Conflicts of Interest: The authors declare no conflict of interest.

References

1. DOE (U.S. Department of Energy). *Plume Persistence Final Project Report*; LMS/ESL/S15233, ESL-RPT-2018-02; Office of Legacy Management: Grand Junction, CO, USA, May 2018. Available online: <https://www.energy.gov/lm/downloads/plume-persistence-final-project-report> (accessed on 13 July 2021).
2. DOE (U.S. Department of Energy). *Monticello Mill Tailings Site Operable Unit III Geochemical Conceptual Site Model Update*; LMS/MNT/S26486; Office of Legacy Management: Grand Junction, CO, USA, July 2020. Available online: <https://www.lm.doe.gov/Monticello/Documents.aspx> (accessed on 13 July 2021).
3. Zielinski, R.A.; Budahn, J.R. Radionuclides in fly ash and bottom ash: Improved characterization based on radiography and low energy gamma-ray spectrometry. *Fuel* **1998**, *77*, 259–267. [[CrossRef](#)]
4. Wollenberg, H.A. Fission-Track Radiography of Uranium and Thorium in Radioactive Minerals. In Proceedings of the 4th International Symposium on Geochemical Exploration, London, UK, 17–20 April 1972. Available online: <https://escholarship.org/uc/item/95k2q1zd> (accessed on 13 July 2021).
5. Kleeman, J.D.; Lovering, J.F. Uranium distribution in rocks by fission-track registration in lexan plastic. *Science* **1967**, *156*, 512–513. [[CrossRef](#)] [[PubMed](#)]
6. DOE (U.S. Department of Energy). *Final Report of the Decontamination and Decommissioning of the Exterior Land Areas at the Grand Junction Projects Office Facility*; DOE/ID/12584-220, GJPO-GJ-13; Grand Junction Office: Grand Junction, CO, USA, September 1995.
7. DOE (U.S. Department of Energy). *Grand Junction Office Site Environmental Report for Calendar Year 2001*; GJO-2002-341-FOS; Idaho Operations Office: Idaho Falls, ID, USA, July 2002.
8. DOE (U.S. Department of Energy). *Riverton Wyoming Final Completion Report*; Albuquerque Operations Office: Albuquerque, NM, USA, December 1991.
9. DOE (U.S. Department of Energy). *2015 Advanced Site Investigation and Monitoring Report Riverton, Wyoming, Processing Site*; LMS/RVT/S14148; Office of Legacy Management: Grand Junction, CO, USA, September 2016. Available online: <https://www.lm.doe.gov/riverton/Documents.aspx> (accessed on 13 July 2021).
10. DOE (U.S. Department of Energy). *Final Remedial Investigation/Feasibility Study for the U.S. Department of Energy Grand Junction (Colorado) Projects Office Facility*; DOE/ID/12584-16, UNC-GJ-GRAP-1; Grand Junction Office: Grand Junction, CO, USA, April 1989.
11. DOE (U.S. Department of Energy). *Final Site Observational Work Plan for the UMTRA Project Site at Riverton, Wyoming*; U0013801; Grand Junction Office: Grand Junction, CO, USA, February 1998. Available online: <https://www.lm.doe.gov/riverton/Documents.aspx> (accessed on 13 July 2021).
12. Dam, W.L.; Campbell, S.; Johnson, R.H.; Looney, B.B.; Denham, M.E.; Eddy-Dilek, C.A.; Babits, S.J. Refining the site conceptual model at a former uranium mill site in Riverton, Wyoming, USA. *Environ. Earth Sci.* **2015**, *74*, 7255–7265. [[CrossRef](#)]
13. DOE (U.S. Department of Energy). *Uranium-Bearing Evaporite Mineralization Influencing Plume Persistence: Literature Review and DOE-LM Site Surveys*; LMS/ESL/S13437, ESL-RPT-2015-05; Office of Legacy Management: Grand Junction, CO, USA, May 2016. Available online: https://www.energy.gov/sites/prod/files/2016/05/f31/AST_S13437.pdf (accessed on 13 July 2021).
14. Vlasova, I.E.; Kalmykov, S.N.; Sapozhnikov, Y.A.; Simakin, S.G.; Anokhin, A.Y.; Aliev, R.A.; Tsarev, D.A. Radiography and local microanalysis for detection and examination of actinide-containing microparticles. *Radiochemistry* **2016**, *48*, 613–619. [[CrossRef](#)]
15. DOE (U.S. Department of Energy). *Long-Term Surveillance and Maintenance Plan for the Grand Junction, Colorado, Site*; LMS/GJT/S02013-1.0; Office of Legacy Management: Grand Junction, CO, USA, April 2021.
16. Severin, K.P. *Energy Dispersive Spectrometry of Common Rock Forming Minerals*; Springer: Dordrecht, The Netherlands, 2004; 225p. [[CrossRef](#)]
17. Noël, V.; Boye, K.; Kukkadapu, R.K.; Li, Q.; Bargar, J.R. Uranium storage mechanisms in wet-dry redox cycled sediments. *Water Res.* **2019**, *152*, 251–263. [[CrossRef](#)] [[PubMed](#)]